AN ELEMENT FREE GALERKIN METHOD FOR THE SIMULATION OF THE FINITE DEFORMATION OF POLIMERIC FOAMS

Guilherme da Costa Machado, gcmachado@emc.ufsc.br
Marcelo Krajnc Alves, krajnc@emc.ufsc.br
Dep. Eng. Mecânica – Gmac, UFSC, CP 476, Florianópolis, SC, 88010-970, Brazil

Hazim Ali Al-Qureshi, hazim@ emc.ufsc.br
Dep. Eng. Mecânica – Gmac, UFSC, CP 476, Florianópolis, SC, 88010-970, Brazil

Rodrigo Rossi, rrossi@ucs.br
Dep. Eng. Mecânica – UCS, Caxias do Sul, RS, 95070-560, Brazil

Abstract. *This work proposes a constitutive model and a numerical scheme, based on the element free Galerkin method, for the simulation of the finite deformation of polimeric foams. The deformation process is subjected to a unilateral contact with friction condition. The proposed model assumes a multiplicative decomposition of the deformation gradient into an elastic and a plastic part, which incorporates a nonlinear hardening behaviour. The constitutive model is written in terms of the logarithm strain and rotated Kirchhoff stress measures. A total Lagrangian formulation of the problem is considered in order to improve the computational performance of the proposed algoritm. The imposition of the essential boundary condition and also of the unilateral contact with friction condition are made by the application of the Agmented Lagrangian method. Some numerical results are presented; under axisymmetric and plane strain conditions, in order to attest the performance of the proposed numerical scheme.*

Keywords*: polymeric foam, element free Galerkin, finite elasto-plasticity, Augmented Lagrangian method*

1. INTRODUCTION

The polymeric foams are more and more used in industry and in domestic applications. Made of a skeleton of more or less regular open or closed cells, here cells are the basic unit of these materials; they have a high energy absorption capacity, particularly useful for shock applications, acoustic and thermal insulating properties, and in some cases, for filtering applications. For these reasons, they are widely used in aircraft and automotive industry, buildings and packaging. Combining good mechanical properties with a low density, rigid polymer foams can also be used as structural materials. Whatever their use, their optimization needs the understanding of their microstructure/macroscopic mechanical property relationships. Indeed, the mechanical response of these materials depends on their architecture, and on the intrinsic properties of the polymer in the cell wall. The architecture is determined by the cell wall thickness, the size distribution and the cells shape. A typical polymeric foam material is illustrated in Fig. 1

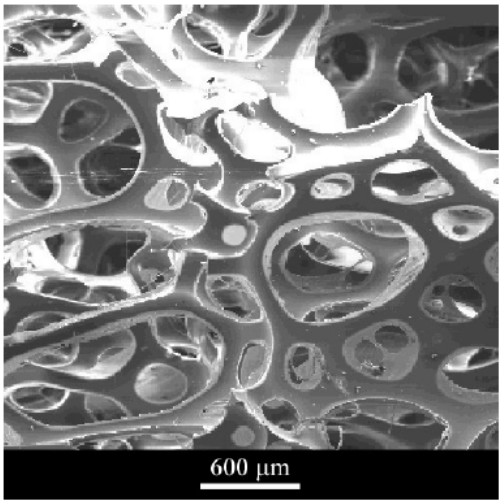

Figure 1. Typical polymeric foam with open cells

Theoretical studies on foam have mainly addressed the behavior of low density foams. The structures of these foams are simulated by a compact assembly of walls and struts. All these models can be divided into two groups: complex modeling approaches based on finite element method which try to describe as finely as possible the foam microstructure; or simpler and more numerous models which largely simplify this microstructure such as Gibson and

Ashaby (1997) and Landro *et al.*(2001). These models are based on the assembly of geometric symmetric cells and relate analytically the elastic material properties and yield stress to the foam relative density. In the case of very high density foams, made of spherical cells that are closed and isolated ones from the others, the materials can be considered as porous.

The useful properties of cellular solids depend on the material from which they are made, their relative density, and their internal geometrical structure. It is important to link the physical properties of cellular solids to their density and complex microstructure, in order to understand how such properties can be optimized for a given application. Thus, for this class of material we consider an elasto-plastic model that incorporates a hyperelastic constitutive relation which depends on the relative density of the material. This dependence is justified for foam structures that experience a large volumetric reduction in a usual compressive process, as show in Roberts and Garboczi (2001, 2002). The plastic phase is described by a modified J_2 model that accounts for the influence of the hydrostatic compression and considers a volumetric and uniaxial compression hardening law.

The adopted formulation considers: a *total Lagrangian* description of the finite deformation problem; a multiplicative decomposition of the deformation gradient, into a plastic and an elastic part; and a constitutive formulation, given in terms of the logarithmic deformation measure, or *Hencky* measure, and the rotated *Kirchhoff* stress.

2. THEORETICAL DEVELOPMENT

Here, we consider a rate-independent plasticity model for the simulation of isotropic polymeric foam materials. Due to experimental observation, a volumetric and a uni-axial compression hardening law is accounted by the model, which also incorporates a different response in compression and tension. In compression the ability of the material to deform volumetrically is enhanced by cell wall buckling processes as described by Gibson & Ashby (1997). It is assumed that the foam cell deformation is not recoverable instantaneously and can, thus, be idealized as being plastic for short duration events. In tension, on the other hand, cell walls break readily; and as a result the tensile load bearing capacity of crushable foams may be considerably smaller than its compressive load bearing capacity. The hardening laws considered by the proposed model assume the evolution of the yield surface is controlled by the volumetric plastic strain experienced by the material.

2.1. Multiplicative decomposition of the deformation gradient

Here, we assume the deformation gradient $\mathbf{F}$ to be decomposed into an elastic deformation, $\mathbf{F}^e$, and a plastic deformation, $\mathbf{F}^p$, as follows

$$\mathbf{F} = \mathbf{F}^e\mathbf{F}^p \tag{1}$$

with

$$\mathbf{F} = \nabla_x \varphi\left(\boldsymbol{X}, t\right), \tag{2}$$

in which $\mathbf{x} = \varphi\left(\boldsymbol{X}, t\right)$ denotes the deformation function. At this point, we define the deformation measure to be the logarithmic or *Hencky* strain tensor, given by $\mathbf{E}^e = \ln\left(\mathbf{U}^e\right)$, where $\mathbf{F}^e = \mathbf{R}^e\mathbf{U}^e$. The conjugate stress measure, for isotropic materials, is given by the *rotated Kirchhoff* stress $\overline{\boldsymbol{\tau}}$,

$$\overline{\boldsymbol{\tau}} = (\mathrm{R}^e)^{\mathrm{T}}\,\boldsymbol{\tau}\,(\mathrm{R}^e), \tag{3}$$

where $\boldsymbol{\tau}$ is the *Kirchhoff* stress, $\boldsymbol{\tau} = \det(\mathrm{F})\boldsymbol{\sigma}$, with $\boldsymbol{\sigma}$ denoting the Cauchy stress, see Peric and Owen (1998).

2.2. Definition of the yield surface

In order to define the yield function, we must introduce the deviatoric rotated Kirchhoff stress, the effective rotated Kirchhoff stress, and the pressure stress, which are respectively as

$$\overline{\boldsymbol{\tau}}^D = \overline{\boldsymbol{\tau}} - \frac{1}{3}\mathrm{tr}\left(\overline{\boldsymbol{\tau}}\right)\mathbf{I}, \quad q = \sqrt{\frac{3}{2}\overline{\boldsymbol{\tau}}^D \,:\, \overline{\boldsymbol{\tau}}^D}\,, \text{ and } \quad p = -\frac{1}{3}tr\left(\overline{\boldsymbol{\tau}}\right). \tag{4}$$

The yield function for crushable foam materials, defined in terms of the Kirchhoff stress, shown in Fig. 2, is given

$$\mathcal{F}(q,p)=\sqrt{q^2+\alpha^2\left(p-\left[\frac{p_c-p_t}{2}\right]\right)^2}-\alpha\left[\frac{p_c+p_t}{2}\right]\leq 0\,, \tag{5}$$

where $\alpha=\alpha\left(\overline{\varepsilon}_k\right)$ and $p_c=p_c\left(\overline{\varepsilon}_k\right)$ are a function of the volumetric compacting plastic strain, $\overline{\varepsilon}_1\equiv\varepsilon_v^p$,

$$\varepsilon_v^p=-\ln\left(J^p\right) \tag{6}$$

where

$$J^p=\det\left(F^p\right)\,, \tag{7}$$

and the axial plastic strain, $\overline{\varepsilon}_2\equiv\varepsilon_a^p$, whose definition, in a unilateral compression test, is given by,

$$\varepsilon_a^p=-\ln\left(\frac{L^p}{L_o}\right)\,, \tag{8}$$

in which L^p is the unloaded length, after the deformation has been applied, and L_o is the length of the initial configuration of the reference specimen.

Here, we consider the hydrostatic tension strength, p_t, to be proportional to the compressive hydrostatic yield stress as $p_t=\zeta p_c$, where ζ represents a constant of proportionality. In general p_t is around 5% to 10% of p_c, see Hanssen *et al.* (2001) and Hallquist (1998).. Moreover, we assume the hydrostatic compression strength, p_c, to evolve as a result of compaction (increase in density) or dilation (reduction in density) of the material, i.e. $p_c=p_c\left(\varepsilon_v^p\right)$. Also, the parameter α is considered to depend on the volumetric compacting plastic strain ε_v^p and also on the axial plastic strain ε_a^p, i.e., $\alpha=\alpha(\varepsilon_v^p,\varepsilon_a^p)$, given in a uniaxial state by

$$\alpha=\frac{\overline{\tau}_y}{\left\{p_t p_c-\frac{1}{3}\overline{\tau}_y\left(p_t-p_c\right)-\frac{1}{9}\overline{\tau}_y^2\right\}^{\frac{1}{2}}}\,. \tag{9}$$

Thus, the parameters, $p_c(\varepsilon_v^p)$ and $\alpha(\varepsilon_v^p,\varepsilon_a^p)$, are sufficient to define the center and the lengths of the major and minor axes of the yield ellipse. These parameters are variables which are functions of the volumetric compacting plastic strain ε_v^p, which describes the so-called consolidation phenomenon, Zhang *et al*. (1998), and on the effective axial plastic strain ε_a^p. The two consolidation variables (α,p_c) are uniquely determined by the knowledge of two experimental tests, given by the uniaxial and hydrostatic compression tests. Thus, $\mathcal{F}=\mathcal{F}(\alpha,p_c)$ where α and p_c are material parameters. Other yield functions have also been proposed in the literature, see Hallquist, (1998) and Deshpande and Flake (2000) for aluminum foams.

2.3. The non-associative plastic flow potential

The plastic modified strain rate for the non associative volumetric hardening model, see Fig. 1, is assumed to be

$$\overline{\mathrm{D}}^p=\dot{\lambda}\frac{\partial\mathcal{G}}{\partial\overline{\boldsymbol{\tau}}}\,, \tag{10}$$

with

$$\mathcal{G}(q,p)=\sqrt{q^2+\beta^2p^2} \tag{11}$$

where β is related to the plastic Poisson's ratio ν_p by

$$\beta = \frac{3}{\sqrt{2}}\sqrt{\frac{1-2\nu_p}{1+\nu_p}}. \tag{12}$$

complemented by postulating a null plastic spin, compatible with plastic isotropy, $\overline{\mathrm{W}}^p = 0$. Here, $\dot{\lambda}$ is the plastic multiplier which must satisfy the Kuhn-Tucker conditions: $\mathcal{F} \le 0$, $\dot{\lambda} \ge 0$ and $\dot{\lambda}\mathcal{F} = 0$.

The usual assumption, for polymeric foams is to consider ν_p = 0.0. In the absence of the knowledge of the plastic Poisson's ratio, the consideration of a zero plastic Poisson's ratio is a reasonable assumption, as shown in Zhang *et al*. (1998), Gibson & Ashby (1997) and Gilchrist & Mills (2001).

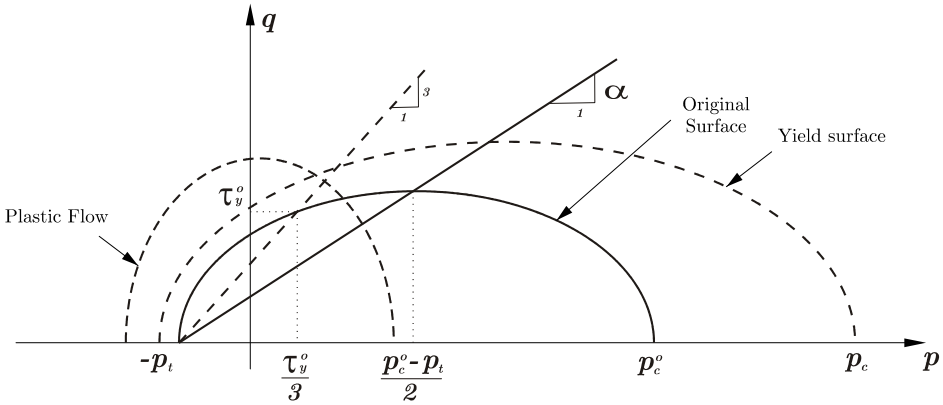

Figure 2. - Yield surface and flow potential on $p - q$ stress space.

2.4. Hyperelastic response

Here, we consider the elastic response to be given, in terms of the logarithmic or *Hencky* strain tensor and the rotated Kirchhoff stress, as

$$\overline{\boldsymbol{\tau}} = \mathbb{D}(\rho^*)\,\mathbf{E}^e, \tag{13}$$

where

$$\mathbb{D}(\rho^*) = 2\mu(\rho^*)\,\mathbb{I} + \left(K(\rho^*) - \frac{2}{3}\mu(\rho^*)\right)(\mathbf{I}\otimes\mathbf{I}) \tag{14}$$

where $\mathbb{D}\left(\rho^*\right)$ is the fourth order elasticity tensor, $\mathbb{I}$ is the fourth order identity tensor, **I** is the second order identity tensor, $K(\rho^*)$ is the bulk modulus, $\mu(\rho^*)$ is the Lamé's coefficient or the shear modulus and ρ^* denoting the relative density, which is defined by the ratio of the foam density, ρ, by the fully compact material density, ρ_M, i.e.,

$$\rho^* = \frac{\rho}{\rho_M}. \tag{15}$$

At this point, writing the continuity equation with relation of relative density we obtain

$$\rho_o^* = \det\left[\mathbf{F}\right]\rho^*, \tag{16}$$

in which $\rho_o^* = \rho_o^*(\boldsymbol{X})$ denotes the initial relative density, defined in the reference configuration, and $\rho^* = \rho^*(\boldsymbol{X}, t)$ the actual relative density, defined at the reference configuration. Now, the proposed model considers

$$\nu(\rho^*) = \nu_o = \text{cte}. \tag{17}$$

and

$$E(\rho^*) = (\rho^*)^\gamma E_M \tag{18}$$

with ν_M representing the Poisson's ratio and E_M the Young's modulus of the fully dense material.

2.5. Hardening Rules

The scalar valued functions $H_a(\varepsilon_a^p)$ and $H_p(\varepsilon_v^p)$ are the hardening functions determined in a uniaxial and hydrostatic compressive tests respectively.

$$\overline{\tau}_y = \overline{\tau}_y^o + H_a(\varepsilon_a^p) \tag{19}$$

and

$$p_c = p_c^o + H_p(\varepsilon_v^p) \tag{20}$$

where, p_c^o is the initial yield compression stress obtained in a hydrostatic test and $\overline{\tau}_y^o$ is the initial yield stress obtained in a uniaxial compression test. Notice that, in a general multiaxial loading we are not able to identify $\overline{\varepsilon}_a^p$. Thus, the axial plastic strain measure must be modified in terms of a new plastic measure that is computable in a general loading case. Now, in a uniaxial compression test we have

$$\varepsilon_a^p = \frac{\varepsilon_v^p}{(1-2\nu_p)}, \tag{21}$$

which will be used in a general framework in order to account for the uniaxial compression hardening test.

2.6. Incremental weak form of the problem

Let $\mathcal{K} = \left\{ \boldsymbol{u} \middle| u_i \in W_s^1(\Omega),\ \boldsymbol{u} = \overline{\boldsymbol{u}} \text{ on } \Gamma_o^u \right\}$, for a sufficiently large s, denote the set of admissible displacements and $\mathcal{V} = \left\{ \delta\boldsymbol{u} \middle| \delta u_i \in W_s^1(\Omega),\ \delta\boldsymbol{u} = \boldsymbol{0} \text{ on } \Gamma_o^u \right\}$ the set of admissible variations. The weak formulation of the problem may be stated as: Find $\boldsymbol{u}_{n+1} \in \mathcal{K}$ so that $\mathcal{F}(\boldsymbol{u}_{n+1}; \delta\boldsymbol{u}) = 0 \quad \forall\, \delta\boldsymbol{u} \in \mathcal{V}$, i.e.,

$$\mathcal{F}(\boldsymbol{u}_{n+1}^k; \delta\boldsymbol{u}) = \int_{\Omega_o} \mathbf{P}\left(\boldsymbol{u}_{n+1}^{h^k}\right) \cdot \nabla_{\boldsymbol{X}} \delta\boldsymbol{u}^h \, d\Omega_o - \int_{\Omega_o} \rho_o \overline{\boldsymbol{b}}_{n+1} \cdot \delta\boldsymbol{u}^h \, d\Omega_o + \int_{\Gamma_o^t} \overline{\boldsymbol{t}}_{n+1} \cdot \delta\boldsymbol{u}^h \, dA_o + \mathcal{F}^u(\boldsymbol{u}_{n+1}^k, \delta\boldsymbol{u}) \tag{22}$$

The imposition of the essential boundary condition is done by the application of the Augmented Lagrangian method, where the term associated with the imposition of the essential boundary conditions is given by

$$\mathcal{F}^u(\boldsymbol{u}_{n+1}^k, \delta\boldsymbol{u}) = -\int_{\Gamma_o^u} \boldsymbol{q}^u\left(\boldsymbol{u}_{n+1}^k, \epsilon_u, \boldsymbol{\lambda}_{u_{n+1}}^k\right) \cdot \delta\boldsymbol{u} \, d\Gamma_o^u \ . \tag{23}$$

where $\boldsymbol{q}^u$ is given by

$$\boldsymbol{q}^u\left(\boldsymbol{u}_{n+1}^k, \epsilon_u, \boldsymbol{\lambda}_{u_{n+1}}^k\right) = -\left[\boldsymbol{\lambda}_{u_{n+1}}^k + \frac{1}{\epsilon_u}\left(\boldsymbol{u}_{n+1}^k - \overline{\boldsymbol{u}}_{n+1}\right) \right]. \tag{24}$$

The Lagrange multipliers are updated as

$$\boldsymbol{\lambda}_{u_{n+1}}^{k+1} = -\left[\boldsymbol{\lambda}_{u_{n+1}}^k + \frac{1}{\epsilon_u}\left(\boldsymbol{u}_{n+1}^k - \overline{\boldsymbol{u}}_{n+1}\right) \right] \tag{25}$$

which shows that the lagrangian multiplier represents physically the traction acting at the essential boundary condition due to the reaction force.

2.7. Discretization by the Element Free Galerkin Method

Recently, a considerable attention has been given to the so-called "meshless methods", which has been applied where the traditional finite element method face difficulties, such as in large deformation problems. Naturally, despite the advantages of these methods, some new problems have originated, such as the need to: implement appropriate numerical integration schemes and enforce essential boundary conditions.

Here, we employ a conventional *Gauss-Legendre* integration scheme, as use in the finite element method and apply the Augmented Lagrangian method, for the imposition of both the unilateral contact with friction and the essential boundary conditions.

2.7.1. Moving least square approximation

The usage of the *Moving Least Square Approximation* enables the construction of an approximate function $u^h(X)$ that fits a discrete set of data $\{u_I, I=1\ldots n\}$, where:

$$u^h(\boldsymbol{X}) = \sum_{I=1}^{n} \Phi_I(\boldsymbol{X}) u_I \tag{26}$$

$$\Phi_I(\boldsymbol{X}) = \boldsymbol{p}(\boldsymbol{X}) \cdot \mathbf{A}(\boldsymbol{X})^{-1} \boldsymbol{b}_I(\boldsymbol{X}) \tag{27}$$

$$\mathbf{A}(\boldsymbol{X}) = \sum_{I=1}^{n} w(\boldsymbol{X} - \boldsymbol{X}_I)\left[\boldsymbol{p}(\boldsymbol{X}_I) \otimes \boldsymbol{p}(\boldsymbol{X}_I)\right] \tag{28}$$

and

$$\boldsymbol{b}_I(\boldsymbol{X}) = w(\boldsymbol{X} - \boldsymbol{X}_I)\boldsymbol{p}(\boldsymbol{X}_I), \tag{29}$$

in which: $\{p_j(\boldsymbol{X}), j=1\ldots m\}$ represents the set of intrinsic base functions; $w(\boldsymbol{X} - \boldsymbol{X}_I)$ is a weight function centered at $\boldsymbol{X}_I$; $\Phi_I(\boldsymbol{X})$ is the derived global shape function, defined at particle $\boldsymbol{X}_I$; and $\mathbf{A}(\boldsymbol{X})$ is the moment matrix, see Liu (2002) and Belytschko *et al.* (1994).

2.7.2. Element-free Galerkin

The objective of the EFG method is to construct a set of global shape functions, $\Phi_I(\boldsymbol{X})$ defined at each particle $\boldsymbol{X}_I$ that defines the approximation space. These global shape functions are then used together with the *Galerkin* method to solve boundary value problems. The particle distribution and the definition of the size of the support of the global base functions aren't arbitrary since they must satisfy the stability condition:

$$card\left\{\boldsymbol{X}_J \,|\, \Phi_J(\boldsymbol{X}) \neq 0\right\} \geq \dim\left[\mathbf{A}(\boldsymbol{X})\right] \tag{30}$$

,i.e., the number of particles $\boldsymbol{X}_J$ whose associated shape function $\Phi_J(\boldsymbol{X})$ have a nonzero value at $\boldsymbol{X}$, must be larger than the size of $\mathbf{A}(\boldsymbol{X})$, which is given by the number of intrinsic base functions in $p(\boldsymbol{X})$. Moreover, for $\boldsymbol{X} \in R^n$, there must be $n+1$ particles, whose position vectors form a nonzero *n-th* rank simplex element, Liu *et al.* (1997). In this work, $X \in R^2$, with $\boldsymbol{X}=(X,Y)$, and the intrinsic base functions is $p^T(\boldsymbol{X})=[1,X,Y]$. Notice that, since the MLSA reproduces exactly the intrinsic base functions in $p(X)$, the consideration of a linear intrinsic base ensures the satisfaction of the classical patch test.

In order to obtain a particle distribution that comply with (30), one performs a partition of the domain, Ω, into a triangular integration mesh, where one considers each triangular partition/element to be an integration cell and each vertex node to be the position of a particle.

2.7.3. Element-free *Galerkin* weight functions

One of the most used weight function is the quartic-spline function, which is given as:

$$w(r) = \begin{cases} 1 - 6r^2 + 8r^3 - 3r^4, & \text{for} \quad r \le 1.0 \\ 0, & \text{for} \quad r > 1.0 \end{cases} \tag{31}$$

in which $r = r_I / \overline{r}_I$ with $r_I = \|\boldsymbol{X} - \boldsymbol{X}_I\|$. The radius $\overline{r}_I$, defining the support of $w(\boldsymbol{X} - \boldsymbol{X}_I)$, is determined by

$$\overline{r}_I = s \cdot r_{I\max}, \qquad s > 1, \quad s \in R \tag{32}$$

with

$$r_{I\max} = \max_i \|\boldsymbol{X}_i - \boldsymbol{X}_I\|, \qquad i \in J_I, \tag{33}$$

where J_I represents the set of adjacent nodes associated with $\boldsymbol{X_I}$. Here, the "optimal" value of s =1.5, was determined from a parametric analysis performed in Rossi and Alves (2004, 2005). An example of the covering of a given domain is illustrated in Fig. 3.

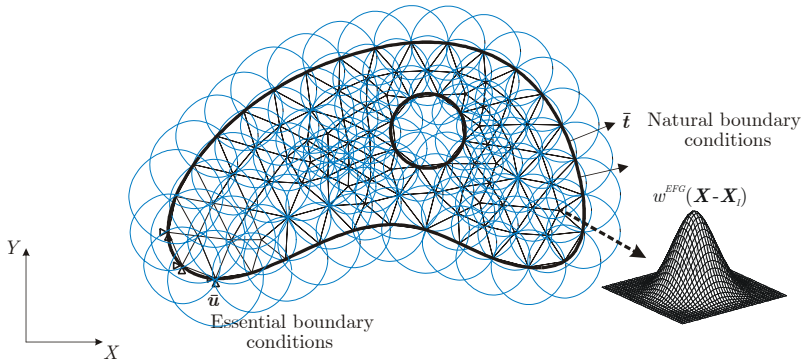

Figure 3 - An example of body coverage by the EFG

Notice that, the EFG global shape functions $\{\Phi_I(\boldsymbol{X}), I=1\ldots n\}$ do not satisfy, in general, the kronecker delta property, i.e., $\Phi_I(\boldsymbol{X_J}) \neq \delta_{IJ}$. As a result, it is not possible to enforce the essential boundary conditions, by directly prescribing nodal values, as done in the FEM. However, there are many possible ways, proposed in the literature, to enforce the essential boundary condition. Among the various possibilities one may mention:

- the usage of Lagrange multiplier methods;
- the usage of collocation methods;
- the formulation of modified variational principles;
- the combination of EFG with FEM;
- the usage of singular weight functions;
- the application of penalty methods;
- the usage of special weight function.

Here, since the most robust strategy presented in the literature to enforce an unilateral contact with friction condition employs the Augmented Lagrangian method, the most natural approach, employed in this work, is to extend the Augmented Lagrangian method to additionally impose the essential boundary condition.

2.8. Numerical results

2.8.1. Uniaxial compression test

Here, the simulation of a uniaxial compression test is presented and confronted with de experimental data obtained in Zhang, J. *et al*. (1998). The specimen has an initial area of 2500mm^2 and 50mm of height. The material parameters used in this analysis are described in Table 1. The process consists is prescribing the displacement of the upper part of the specimen, with a total upsetting of u_y = 30mm, applied in order to compress the body. Due to the axisymmetry condition, only half of the domain is modeled. This example uses an integration mesh with 4 triangular cells and 9 EFG particles. A support of influence of s=1.5 together with a 7 points integration *Gauss-Legendre* scheme is employed in the analysis. In addition, an external penalty parameter of $\epsilon_u = 10^{-6}$.is used in the analysis.

Table 1 – Material Parameters.

$\tau_y^o = 82,034\ KPa$	$E_m = 928,092\ MPa$	$\nu = 0,25$
$p_c^o = 40,470\ KPa$	$\rho_o^* = 0,049$	$\gamma = 1,54$
$\zeta = 0,30$	$\nu_p = 0,00$	$c = 0,30$

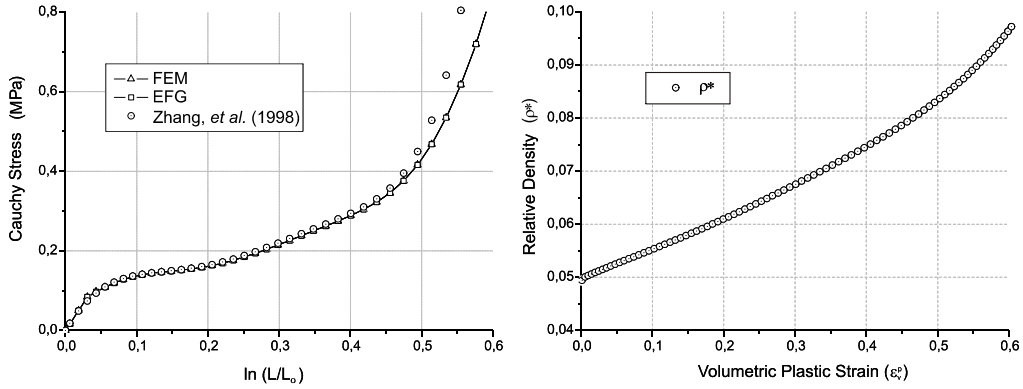

(a) (b)

Figure 4- Uniaxial simulation: (a) Cauchy Stress versus the logarithm strain; (b) Variation of relative density with respect the volumetric plastic strain.

2.8.2. Conical slab

This example considers an axisymmetric problem that consists in the upsetting of a conical slab, whose dimensions are: r_1=90*mm*; r_2=45*mm*; h=100*mm*. The analysis consists in prescribing the displacement of the upper wall, with a total upsetting of u_y=80*mm*, which was applied in 1000 step-loads, in an integration mesh with 240 cells and 143 EFG particles. The parameters used in this analysis are the same presented in Table 1. Again, 7 points integration *Gauss-Legendre* scheme is used, as well the support of influence s=1.5 and the penalty parameter ϵ_u =10^{-6}.

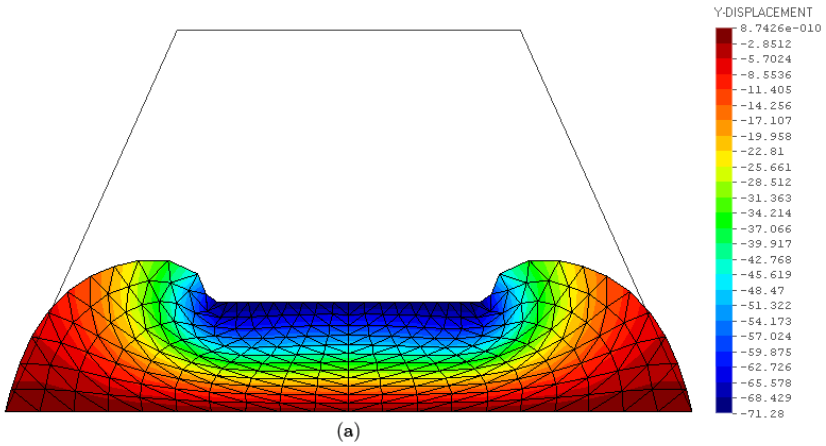

(a)

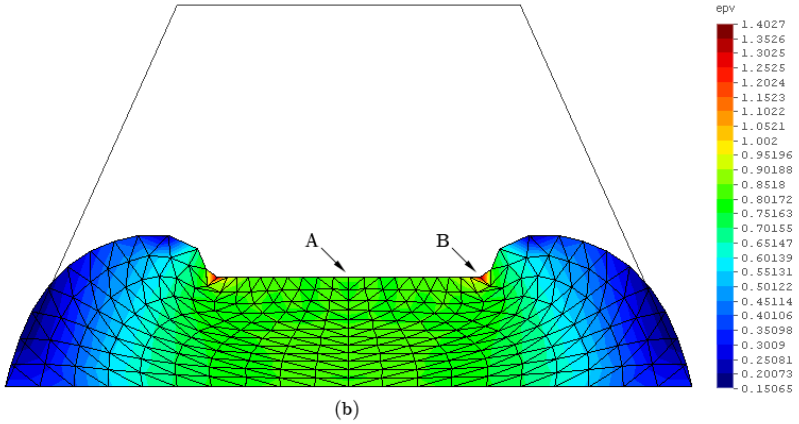

(b)

Figure 5- Fringes results from: (a) displacement on *y* direction, u_y; (b) volumetric plastic strain, ε_v^p .

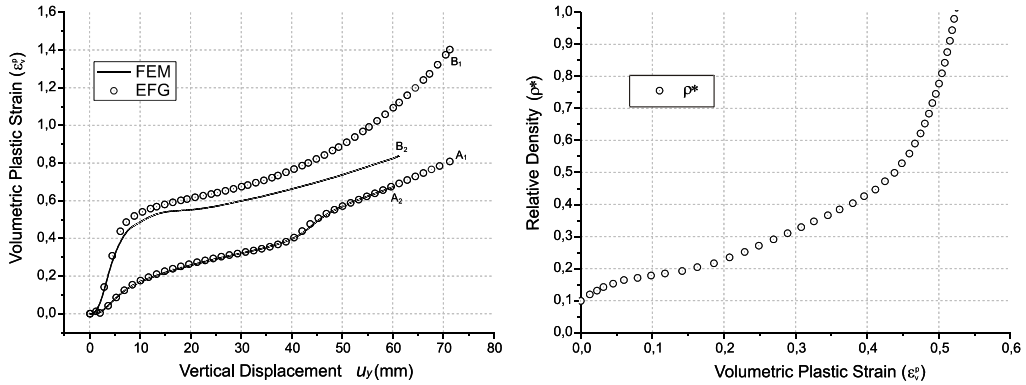

(a) (b)

Figure 6- Uniaxial simulation: (a) Cauchy Stress versus the logarithm strain. The indexes A and B refers to the points indicated in Figure 5 and the sub indexes 1 and 2 refers to FEM and EFG methods respectively; (b) Variation of relative density with respect the volumetric plastic strain.

2.8.3. Indentation

In this example is presented an identation test, under plane strain conditions. The initial dimensions of the body and also of the tool are shown in Fig. 7.

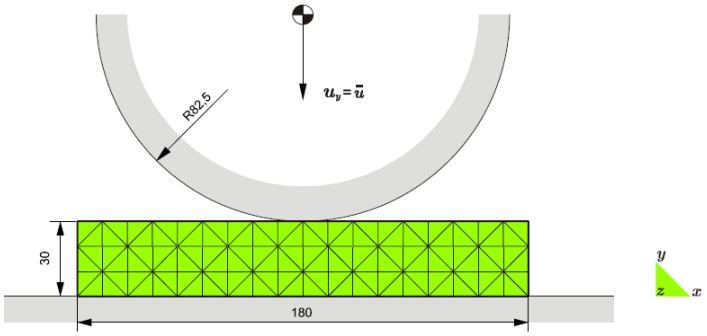

Figure 7. Definition of the problem (dimensions in *mm*)

The simulation consists in prescribing a total upsetting of the tool of $\bar{u} = -15$ mm in 1000 displacement increments. The upper and lower surfaces are subjected to a unilateral contact with friction condition. The domain is discretized by 108 cells with 76 particlesusing a 7 points integration scheme. The data employed in the analysis are: $c_f = 0.1$, $\varepsilon_v = 10^{-4}$, $\varepsilon_T = 10^{-3}$ and $\varepsilon_u = 10^{-6}$.

The deformed configuration together with the displacement field is illustrated in Fig. 8,

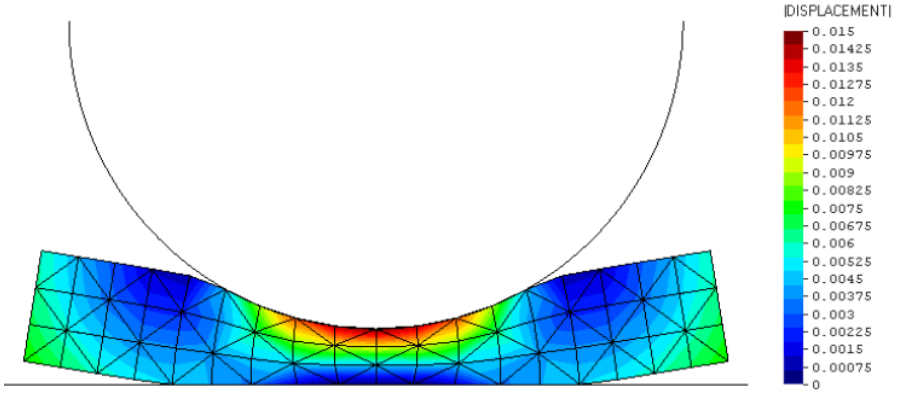

Figure 8 – Deformed configuration and the displacement field in *(mm)*

The deformed configuration and the relative density field of the material is illustrated in Figure 9,

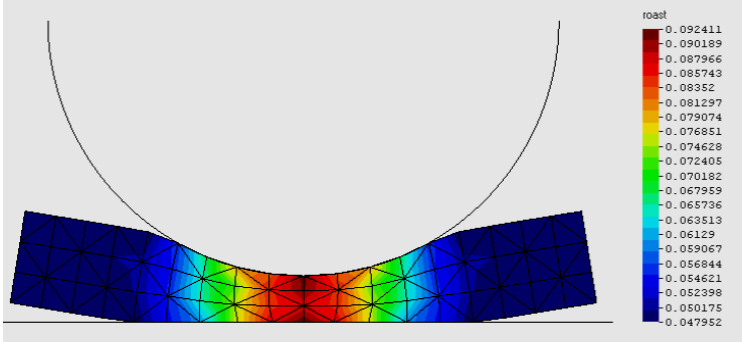

Figure 9 – Distribution of the relative density of the material

2.9. Discussion and conclusion

Polymeric foam constitutive behavior is extremely complex on the microstructural scale. Cellular buckling under compression initiates a long stress plateau. Further compression causes stress bottom up due to foam consolidation. Thus, adequate modeling of foam materials is still a challenge. Most of the problems are due to inadequate modeling of the elastic behavior of the material. The proposed model showed reasonably prediction for the responses of rigid polymeric foams under the monotonic loading conditions. Non monotonic loading must be further investigagted.

One of the most relevant advantages in use the element-free Galerkin method, compared with the FEM, is the ability of the method to withstand the analysis of very large deformation processes, with no remeshing, without breaking up. In addition, EFG method showed to be more robust to capture high deformation and deformation gradients, in which the material is subjected to a huge densification process, as shown in curves *B1* and *B2* in Fig. 6, where the FE solution breaks up before the EFG solution.

3. ACKNOWLEDGEMENTS

The support of the CNPq and Multibras S.A. is gratefully acknowledged.

4. REFERENCES

Belytschko, T., Lu, Y.Y., Gu, L., 1994, “Element free Galerkin methods’, International Journal for Numerical Methods in Engineering, Vol.37, pp. 229-256.

Deshpande V., Flake N.A. 1999 , “Isotropic constitutive models for metallic foams’, Journal of the Mechanics and Physics of Solids Vol.48, pp. 1253-1283.

Gibson L.J., Ashby M.F., 1997, “Cellular Solids: Structure and Properties”, Cambridge University Press.

Gilchrist A., Mills N.J., 2001, “Impact deformation of rigid polymeric foams: experiments and FEA modeling”, International Journal of Impact Engineering Vol.25, pp. 767-786.

Hallquist, J.O., 1998, “Theoritical Manual of LsDyna”, Livermore Software Technology Corporation.

Hanssen A.G., Hopperstad O.S., Langseth H., Ilstad H., 2001, “Validation of constitutive models applicable to aluminum foams”, International Journal of Mechanical Sciences.

Landro L., Sala G., Olivieri D., 2001, “Deformation mechanisms and energy absorption of polystyrene foams for protective helmets”, Polymer Testing Vol.21, pp. 217-228.

Liu, G.R., 2002, “Mesh Free Methods: moving beyond the finite element method”, CRC Press.

Peric D., Owen D. R. J., 1998, “Finite-element applications to the nonlinear mechanics of solids”, Reports on Progress in Physics, Vol. 61, pp. 1495-1574.

Roberts, A.P., Garboczi E.J., 2002, “Elastic properties of model random three-dimensional open-cell solids”, Journal of the Mechanics and Physics of Solids, Vol. 50, pp.33-55.

Roberts, A.P., Garboczi E.J., 2001, “Elastic moduli of model random three-dimensional closed-cell cellular solids”, Acta Materialia, Vol.49, pp.189–197.

Rossi, R., Alves, M.K., 2004, “Recovery Based Error Estimation and Adaptivity Applied to a Modified Element-Free Galerkin Method”, Computational Mechanics, Vol. 33, n. 3, pp. 194-205

Rossi, R., Alves, M.K., 2005, “An h-adaptive modified element-free Galerkin method”, European Journal of Mechanics, A/Solids, Vol. 24, pp. 782-799.

5. RESPONSIBILITY NOTICE

The authors are the only responsible for the printed material included in this paper.